Pharm Res (2015) 32:1493–1504
DOI 10.1007/s11095-014-1555-4

RESEARCH PAPER

Population Pharmacokinetic Modelling of Irosustat in Postmenopausal Women with Oestrogen-Receptor Positive Breast Cancer Incorporating Non-Linear Red Blood Cell Uptake

Zinnia P. Parra-Guillen • Josep María Cendrós Carreras • Concepción Peraire • Rosendo Obach • Joan Prunynosa • Eric Chetaille • Iñaki F. Trocóniz

Received: 18 March 2014 / Accepted: 17 October 2014 / Published online: 30 October 2014

ABSTRACT

Purpose Irosustat is the 'first-in-class' irreversible potent steroid sulphatase inhibitor with lack of oestrogenic activity. The objective of this work was to develop a population model characterizing simultaneously the pharmacokinetic profiles of irosustat in plasma and whole blood.

Methods This clinical study was an open label, multicentre, phase I multiple cohort dose escalation trial conducted in 35 postmenopausal women with oestrogen-receptor positive breast cancer. Patients received 1, 5, 20, 40, or 80 mg oral doses. Irosustat was administered as a single oral dose to each patient followed by an observation period of 7 days. On day 8 each patient received once daily oral administration until day 34. Concentrations of irosustat in both blood and plasma were obtained and pharmacokinetic analyses were performed with NONMEM 7.2.

Results and Conclusions Irosustat showed non-linear disposition characteristics modelled as maximum binding capacity into the red blood cells. Plasma concentration corresponding to half of the maximum capacity was 32.79 ng/mL. The value of the blood to plasma concentration ratio in linear conditions was 419, indicating very high affinity for the red blood cells. Apparent plasma and blood clearances were estimated in 1199.52 and 3.90 L/day, respectively. Pharmacokinetics of irosustat showed low-moderate inter-subject variability, and neither the demographics (e.g., age, or weight) nor the phenotypes for CYP2C9, CYP2C19, and CYP3A5 enzymes showed statistically significant effects. Relative bioavailability was decreased as the administered dose was augmented. The model predicted a 47% decrease in relative bioavailability in the 40 mg with respect to the 1 mg dose.

KEY WORDS anticancer drugs · non-linear pharmacokinetics · NONMEM · population pharmacokinetics

ABBREVIATIONS

A_{Depot}	Amount of irosustat in the depot (absorption) compartment
AGE	Age
AIC	Akaike information criterion
A_{MAX}	Maximum binding capacity of the red blood cells
A_P	Free amount of irosustat (outside the red blood cells) in blood
A_{RBC}	Drug amount in red blood cells
bql	Below quantification limit
BPR	Blood to plasma ratio
C_B	Blood irosustat concentration
CL_B	Apparent total blood clearance
CL_P	Apparent total plasma clearance
C_P	Plasma irosustat concentration
F_I	Absolute bioavailability
F_H	(unknown) Fraction of the absorbed dose that is lost during the first pass through the liver
HCT	Hematocrit
k_A	First order rate constant of absorption
K_D	Amount of drug required to achieve 50% of A_{MAX}
k_{el}	First order rate constant of elimination
k_{TR}	First order rate constant of transit between compartments
MTT	Mean transit time

Electronic supplementary material The online version of this article (doi:10.1007/s11095-014-1555-4) contains supplementary material, which is available to authorized users.

Z. P. Parra-Guillen • I. F. Trocóniz (✉)
Department of Pharmacy and Pharmaceutical Technology, School of Pharmacy, University of Navarra, Pamplona 31080, Spain
e-mail: itroconiz@unav.es

J. M. Cendrós Carreras • C. Peraire • J. Prunynosa
Pharmacy and Pharmaceutical Technology Department, University of Barcelona, Avda. Joan XXIII s/n, 08028 Barcelona, Spain

R. Obach
Calle Sabino Arana 58 11° 1ª, Barcelona 08028, Spain

E. Chetaille
Ipsen Innovation, Les Ulis, France

NTC	Number of transit compartments
pcVPCs	Prediction-corrected visual predictive checks
Q_H	Liver blood flow
RBC	Red blood cells
SLP	Parameter corresponding to the ratio between A_{MAX} and K_D
V_B	Apparent blood volume
V_P	Apparent plasma volume
WGT	Body weight

INTRODUCTION

Breast cancer is the most common female cancer with around 1.38 million individuals diagnosed worldwide each year, and a lifetime risk of developing the disease of around 1 in 8 women (1, 2). Despite the significant progress in the treatment, worldwide around 458,000 women are still expected to die annually as a consequence of the disease (1).

Almost two thirds of all breast tumours are oestrogen receptor (ER)-positive and their growth is stimulated by oestrogen levels. Selective ER modulators have been the mainstay of hormonal therapy in ER-positive breast cancer in postmenopausal women for the last 30 years (3). The major disadvantage of selective ER modulators is the associated risk of developing endometrial cancer and cardiovascular adverse effects. Therefore, attention has shifted towards drugs that can prevent the formation of oestrogens rather than blocking their effect in target tissues. In postmenopausal women, oestrogens are formed via two routes: the aromatase-catalysed conversion of androstenedione (adione) to oestrone (E1) and the steroid sulphatase (STS) conversion of oestrone sulphate (E1S) to E1 (4). Whilst the aromatase inhibitors (AIs) have become the standard of care in first line metastatic breast cancer, there is a growing unmet medical need for those patients who do not respond or progress whilst receiving AIs (5).

Studies indicate that as much as 10 times more E1 may originate via the sulphatase route than via the aromatase pathway (6–9). Furthermore, STS also regulates the conversion of dehydroepiandrosterone sulphate to dehydroepiandrosterone, which can be reduced to androstenediol (adiol). *In vitro* studies have shown that adiol can bind to the ER and stimulate the growth of ER-positive breast cancers (10,11). Thus the administration of an STS inhibitor could not only prevent the synthesis of E1 but also prevent the formation of tumour-growth-supporting adiol. Recently, a number of studies have confirmed that a high level of STS mRNA expression in tumours is associated with a poor prognosis in women with breast cancer (5,12).

Irosustat (BN83495), a tricyclic coumarin based sulphamate (6-oxo-8,9,10,11-tetrahydro-7H-cyclohepta-[c][1]benzopyran-3-O-sulphamate) is the 'first-in-class' irreversible potent STS inhibitor undergoing clinical activity with lack of oestrogenic activity (13,14). Irosustat inhibited the conversion of E1S to E1 in rat placental microsomes *in vitro* with an IC50 of 8 nM, and following oral administration in rats, a single dose of 1 mg/kg produced >90% inhibition of STS in rat liver whilst five daily doses of 0.1 mg/kg gave 84% inhibition (13). Irosustat was also shown to inhibit the *in vivo* growth of MCF-7 tumours in mice or NMU-induced mammary tumours in rats.

Regarding irosustat biopharmaceutical and pharmacokinetic properties, the compound exhibits low aqueous solubility in the pH range of 1.2–6.8, but high permeability, thus being classified as a class II compound according to the biopharmaceutical classification system. In blood, more that 97% of irosustat is bound to serum proteins, mainly albumin with smaller contributions from α1-acid glycoprotein, transferrin and γ-globulin. Elimination of irosustat is mainly due to metabolism, with a percentage of irosustat dose excreted in urine ranging from 0.006 to 0.287% in patients treated with a single oral dose of 1 to 80 mg. The major cytochrome P450 enzymes involved in the transformation of irosustat were CYP2C8, 2C9, 3A4/5 and 2E1, being glucuronide and sulfate conjugates the main metabolites (15). In addition, slight inhibition of CYP2C19 has been observed in human hepatocytes (16).

Recently, the efficacy and safety results of a phase I dose escalation study aiming to determine the recommended optimal biological dose (RD) of irosustat in postmenopausal women with estrogen receptor-positive breast cancer have been published (17). Irosustat was well tolerated, being dry skin the most frequent adverse event. After 28 days of daily administration of irosustat, most of the patients achieved ≥95% STS inhibition in peripheral blood mononuclear cells and corresponding endocrine suppression. The RD was established at 40 mg dose. The median time to disease progression in the 40 mg cohort was 11.2 weeks.

The objective of the current analysis is to develop a population model characterizing simultaneously the pharmacokinetic profiles of irosustat in plasma and blood after single and repeated oral administration in postmenopausal women with estrogen receptor-positive breast cancer, quantifying the magnitude of the inter-subject and residual variability, and identifying the patient characteristics including genotypes of the relevant liver metabolic enzymes (CYP2C9, CYP2C19, CYP3A5) that might have a significant impact on its pharmacokinetics and might reduce the magnitude of the inter-subject variability (ISV).

This population analysis is of special relevance due to the non-linear pharmacokinetic characteristics of irosustat with regard to the disposition into red blood cells as it has been previously shown both in *ex vivo* and *in vivo* experiments (18).

MATERIAL AND METHODS

Study Design

An open label, multicentre, phase I multiple cohort dose escalation study with once daily oral administration of BN83495 (irosustat) was conducted in postmenopausal women with oestrogen-receptor positive breast cancer. A detailed description of the main features of the study design and patient population is presented elsewhere (17).

Briefly, postmenopausal women over the age of 18 years, whose disease progressed after prior hormonal therapy for ER-positive locally advanced, or metastatic breast cancer, were included in the trial. Patients had to have had satisfactory renal, hepatic and bone marrow functions and a life expectancy of at least 12 weeks. Patients were excluded if they had progressive central nervous system metastasis or inflammatory breast cancer. Further exclusion criteria included but were not limited to patients with cardiac risk factors, malabsorption, concomitant use of coumarin like drugs, or previous cancer treatment within 1 month.

Thirty five cancer patients were recruited into each of the following dose cohorts: 1 ($n=3$), 5 ($n=7$), 20 ($n=6$), 40 ($n=13$), and 80 ($n=6$) mg. Table I lists the individual characteristics of the cancer patient population.

Table I Summary of Patient Characteristics

Patient Characteristics	Patients	Median	Range
Demographics			
Weight (kg)	35	74	55–96
Age (years)	35	65	49–81
Patient status			
WHO performance status (0/1/2/3)	21/14/0/0	–	–
Prior radiotherapy (Yes/No)	11/24	–	–
Biochemical parameters			
Albumin (g/L)	35	39	30–47
Alkaline phosphatase (U/l)	35	99	45–469
Creatinine Clearance-Cockcroft-Gault (mL/s)	35	1.43	0.73–2.24
Gamma GT (U/l)	35	39	12–324
Lactate dehydrogenase (U/l)	35	279	102–746
Serum glutamic oxaloacetic transaminase (U/l)	35	29	16–64
Serum glutamic pyruvic transaminase (U/l)	35	23	11–80
Total bilirubin (μmol/L)	35	8	3.4–21
Total protein (g/L)	35	72	33–82
Triglycerides (mg/mL)	35	1.32	0.56–3.28
Red Blood Cells Count ($\times 10^{12}$/L)	35	4.2	2.91–5.37
Haemoglobin, (g/L)	35	130	100–167
White Blood Cells Count ($\times 10^{9}$/L)	35	5.9	3.5–10.4
Neutrophils ($\times 10^{9}$/L)	35	3.4	1.7–8.6
Lymphocytes ($\times 10^{9}$/L)	35	1.3	0.7–2.73
Platelets ($\times 10^{9}$/L)	35	265	177–448
Hematocrit (L/L)	35	0.37	0.29–0.48
Pharmacogenetics			
Phenotype CYP2C9 (EM/IM/PM)	5/22/8	–	–
Phenotype CYP2C19 (EM/IM/PM)	5/28/2	–	–
Phenotype CYP3A5 (EM/IM/PM)	5/5/25	–	–

EM, IM, PM, extensive, intermediate, and poor metabolizers, respectively

Drug Administration

Irosustat, supplied as powder-filled opaque capsules, was administered as a single oral dose to each patient followed by an observation period of 7 days. On day 8 each patient received once daily oral administration of irosustat until day 33–35. Thus, most patients received a total of 29 oral administrations of irosustat. Two patients in the 1 mg dose group received 28 administrations. In the 5 mg dose group one patient received only the first dose, other patient got 16 oral doses, and two patients received 30 doses. Lastly, in the 40 mg dose group two patients received 27 and 30 oral doses of irosustat, respectively.

Sample Collection

Blood samples to determine the concentration of irosustat in both blood and plasma were obtained at the following times after the first administration: 5 min, 10 min, 15 min, 30 min, 1 h, 2 h, 3 h, 5 h, 8 h, 24 h, 3 days, 5 days and 7 days. The sampling times corresponding to the last day of administration were 10 min, 30 min, 1 h, 2 h, 3 h, 5 h, 8 h, and 24 h after last dose. Additional samples were withdrawn before administration at days 15, 22, and 35.

Analytical Determination of Irosustat in Blood and Plasma

Blood samples (4 mL blood) were collected in sodium heparin tubes. After sampling, the tubes were placed in an ice-water bath. For blood measurements, two aliquots of 0.3 mL blood were taken, and 0.7 mL of 50% formic acid solution was added to each aliquot in order to produce the lysis of the erythrocytes and release of irosustat. These whole blood aliquots were mixed and stored below −70°C until analysis. With respect to total plasma concentration, the remainding blood was kept in sodium heparin tubes in the ice-water bath and was centrifuged (within the next 2 h) at approximately 2,000 g during 15 min at 4°C. The plasma was stored below −70°C until analysis. Irosustat stability was investigated and confirmed during the processing conditions and storage for both, plasma and blood samples.

Concentration values of irosustat in plasma and blood were determined by on-line solid phase extraction attached to liquid chromatography and followed by tandem mass spectrometry (on-line SPE-LC-MS/MS) using a 13C labelled analogue of irosustat as internal standard. For plasma measurements, intra-assay and inter-assay precision data of quality control samples was ranging between 1.21% and 11.70% (intra) and between 3.47 to 9.92% (inter) for the overall data. Intra-assay and inter-assay accuracy data in human plasma was ranging between −15.08% and 6.56% (intra) and between −7.27 to −0.49% for the overall data. The limit of quantitation was established as 0.05 ng/mL. Similarly, intra-assay and inter-assay precision data of quality control samples in human whole blood was ranging between 1.26% and 7.19% (intra) and between 2.67 to 6.04% (inter) for the overall data. Intra-assay and inter-assay accuracy data of quality control samples in human whole blood was ranging between −5.01 and 6.00% (intra) and between −3.48 to −0.17% (inter) for the overall data. The limit of quantification was established as 0.1 ng/mL. Neither relevant matrix effect nor carry-over effect was observed, and a 10-fold dilution or 500-fold dilution on a sample of 500 ng/mL had no significant effect on the levels of irosustat found both in human whole blood and plasma. Consequently, this method was shown to be suitable for measurement of human plasma and blood irosustat concentrations ranging from 0.050 ng/mL to 100 ng/mL, and 0.1 ng/mL to 100 ng/m, respectively.

Brief Description of the Data

A total of 1,438 values of irosustat concentration were obtained, 41 of those were reported as below the limit of quantification (blq). The percentage of blq samples represented less than 3% of the whole blood and plasma data and those samples were ignored. 76 plasma samples were reported as highly hemolyzed. Hemolyzed samples were distributed evenly across the different dose groups and were not considered for the analysis. Therefore, a final number of 1,321 samples, 610 in plasma and 711 in blood, were considered for the subsequent analysis.

Figure 1a shows blood (C_B) and plasma (C_P) irosustat concentration *vs* time profiles corresponding to the first and last administration. In Fig. 1b the relationship between C_B and C_P is represented. Both figures show that irosustat presents non-linear pharmacokinetic characteristics. The levels of irosustat in blood is similar between the 40 and 80 mg dose groups suggesting a limited distribution capacity of the red blood cells.

Data Analysis

The population approach was applied for all analyses using the software NONMEM version 7.2 (19) with the stochastic approximation expectation maximization (SAEM) algorithm followed by Importance sampling (IMP). ISV and inter-occasion (20) (IOV) variability were modelled exponentially. Three occasions were considered: (i) occasion 1, first dose followed by the observation time until day 7; (ii) occasion 2, daily dose administration from day 8 until day 33–34, and (iii) occasion 3 last dose administration. Concentration data in plasma and blood were logarithmically transformed for the analysis and residual variability was described with an additive error model. Different magnitudes of residual errors were estimated for plasma and blood. Observations obtained in plasma and in blood were fit together, that is, a model integrating both type of observations was developed.

Model Selection

Selection between models was based mainly on the inspection of goodness of fit plots and the precision of the parameter estimates. The minimum value of the objective function provided by NONMEM that is approximately equal to -2xlog likelihood (−2LL), served as a guide during model building. Two nested models can be directly compared using the log-likelihood ratio test (LRT) based on the difference of -2LL between the two models. LRT is assumed to be χ^2 distributed (degrees of freedom, df, equal to the number of differing parameters), and therefore a difference in -2LL of 3.84 and 6.63 corresponds to the <0.05 and <0.01 significance levels respectively for one extra model parameter (df=1). When nested models differ in two parameters (df=2), a value of 5.99 is needed for a 0.05 level of significance. For non-nested models the Akaike information criterion was used (AIC) (21). Model parameter estimates are presented together with their coefficients of variation [CV(%)] computed from the results of the covariance step in NONMEM. The degree of ISV and IOV was also expressed as CV(%). The magnitude of residual error was expressed as log(ng/mL).

Model Development

Three steps were followed. First the base population model was built. Then, the selection of significant covariates was performed, and finally the selected model was evaluated.

Base population model building. A population model which in absence of covariates provides a proper description of the data was developed. Both the structural and the statistical parts of the population model were selected at that step. With respect to the latter, the significance of the off-diagonal elements of the **Ω** variance co-variance matrix was explored.

In the following, the structural part of the selected model is described, however during the model building

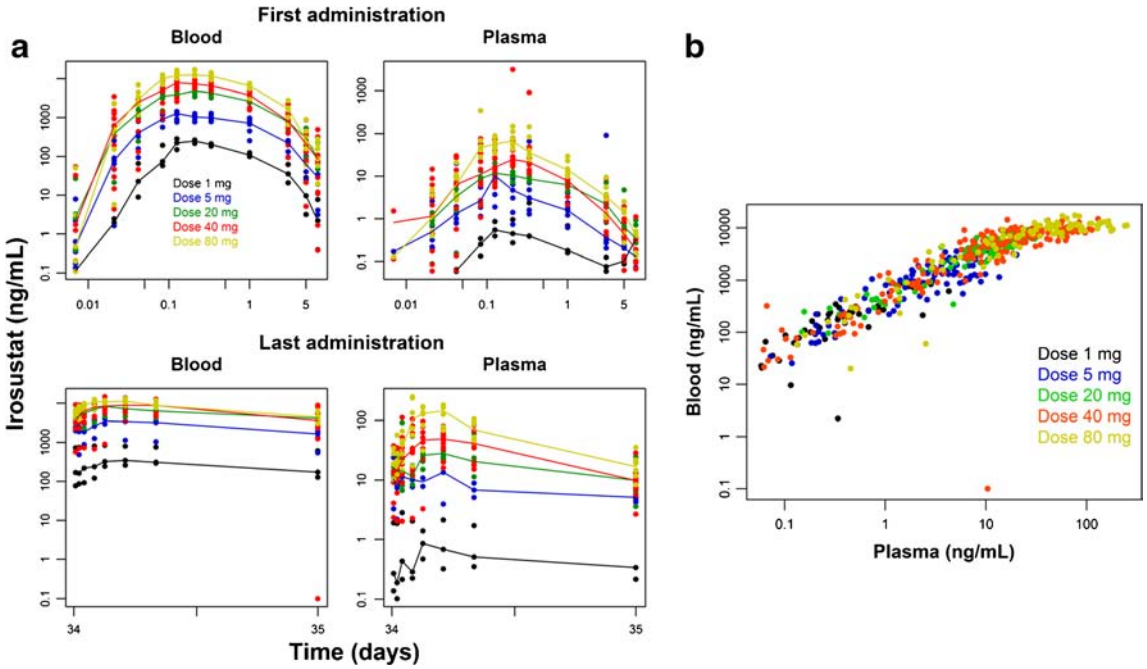

Fig. 1 Raw data *vs* time profiles. (**a**) Measured plasma (*right*) and blood (*left*) irosustat concentrations (*points*) obtained after the first and last admnistrations, and median of the data (*lines*) represented by the dose level administered. (**b**) Blood *versus* plasma raw concentration relationship. The log-log scale were used to facilitate visual inspection in panels (**a**) and (**b**).

process variants of the final model were tested as it is described in the results section. Figure 2 represents the selected model together with the corresponding model parameters.

(i) With respect to the drug absorption process, the transit compartments absorption model was used (Eq. 1) (22). This model represents a generalization of the first order absorption model, increasing flexibility and providing a more physiological interpretation for the process of latency.

$$\frac{dA_{Depot}}{dt} = F_1 \times D \times k_{TR} \times \frac{(k_{TR} \times t)^{NTC} \times e^{-k_{TR} \times t}}{NTC!} - k_A \times A_{Depot} \quad (1)$$

dA_{Depot}/dt accounts for the rate of change in the amount of irosustat in the depot (absorption)

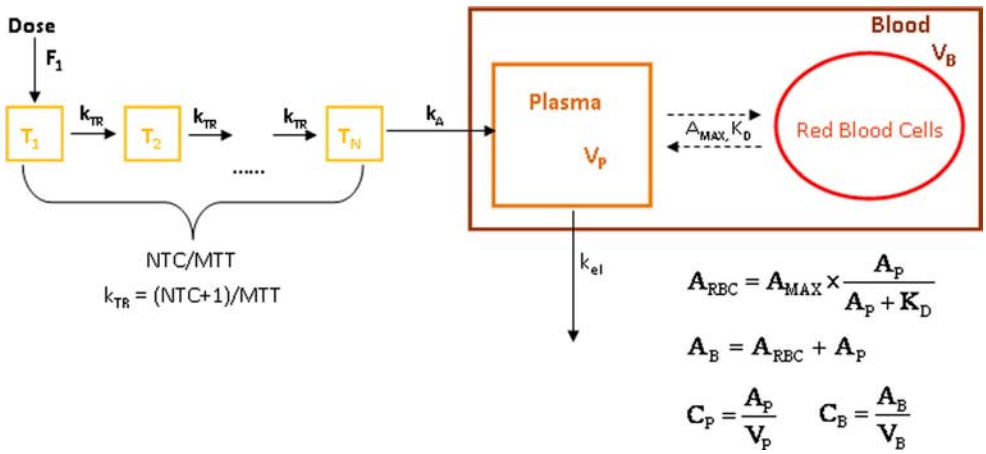

Fig. 2 Schematic representation of the final mathematical model developed for irosustat in blood and plasma. A_P, A_{RBC} and A_B represent the amount of irosustat free (in plasma), bound to the red blood cells (RBC) and in blood (total amount), respectively; V_P and V_B are the apparent plasma and blood volumes of distribution respectively; C_P and C_B represent the concentration of irosustat in plasma and in blood, respectively; F_1 is the (unknown) relative bioavailability; k_{TR} is the first order rate constant of transit between absorption compartments ($T_1 \ldots T_N$); k_A is the first order rate constant of absorption; NTC is the number of transit compartments being the last compartment; TN, the depot compartment; MTT is the mean transit time between compartments; k_{el} is the first order rate constant of elimination; A_{MAX} is the maximum binding capacity of irosustat to RBC and K_D represents the amount of drug required to achieve 50% of A_{MAX}. *Dashed lines* represent instantaneous processes.

compartment (A_{Depot}). At time (t) of the start of the treatment (t=0) $A_{Depot}=F_1 x D$, where F_1 is the bioavailability and D the dose administered. The parameter k_{TR} represents the first order rate constant of transit between compartments and is a derived parameter calculated as (NTC+1)/MTT, where NTC is the number of transit compartments, and MTT the mean transit time. Finally, k_A is the first order rate constant of absorption, and NTC!, is the factorial of NTC that was approximated using the Stirling's formula: $NTC! = \sqrt{2 \times \pi} \times NTC^{NTC+0.5} \times e^{-NTC}$. Therefore Eq. 1 can be expressed as:

$$\frac{dA_{Depot}}{dt} = F_1 \times D \times k_{TR} \times \frac{(k_{TR} \times t)^{NTC} \times e^{-k_{TR} \times t}}{\sqrt{2 \times \pi} \times NTC^{NTC+0.5} \times e^{-NTC}} - k_A \times A_{Depot} \quad (2)$$

To characterize multiple doses, complete absorption between dose administrations was assumed and time was consistently updated to account for time after the last dose administration.

(ii) Regarding drug disposition in the body, the model assumes that distribution of irosustat from plasma to red blood cells (RBC) is an instantaneous and reversible process that occurs in the apparent blood volume (V_B), and that RBC have a limited distribution capacity, characterized by a maximum binding capacity (A_{MAX}) and a K_D, representing the amount of drug required to achieve 50% of A_{MAX}. Drug elimination occurs from the plasma (central compartment) following a first order rate process represented by k_{el}. Given the existence of different volumes of distribution for the different drug processes (i.e., elimination, binding between the drug in plasma and red blood cells), amounts, rather than concentrations, were used to express binding capacity.

Equation 3 represents the rate of change of the free amount of irosustat (outside the red blood cells) in blood (A_P), dA_P/dt. The model is based in the model described previously by Wagner (23) and it has been applied in several occasions (24,25).

$$\frac{dA_P}{dt} = \frac{k_A \times A_{Depot} - k_{el} \times A_P}{1 + \frac{A_{MAX} \times K_D}{(A_P + K_D)^2}} \quad (3)$$

The drug amount in red blood cells (A_{RBC}) follows a Michaelis-Menten kinetics as it is represented by the following expression (Eq. 4):

$$A_{RBC} = \frac{A_{MAX} \times A_P}{K_D + A_P} \quad (4)$$

Therefore, C_P is obtained as A_P/V_P, where V_P, is the apparent volume of distribution of the plasma (central) compartment assuming that, for practical purposes, all the concentration of irosustat in plasma is unbound. Finally C_B is calculated as the total amount of drug in the system (A_P+A_{RBC}) divided by V_B.

Under these conditions, and based on Wagner derivations (23), the terminal half-life can be calculated as follows:

$$\lambda_z = \frac{k_{el}}{1 + \frac{A_{MAX}}{K_D}} \quad (5)$$

The following set of typical population parameters were estimated during the analysis: MTT, NTC, k_A, V_P, V_B, k_{el}, A_{MAX}, and K_D. With respect to bioavailability (F_1), since intravenous data were not available the typical estimate was fixed to 1 (but ISV and IOV on F_1 were allowed), and therefore V_P and V_B should be considered as apparent volumes of distributions (V_P/F_1, and V_B/F_1, respectively).

Covariate selection. The covariates are listed in Table I. In a first step, correlation between covariates was evaluated, when a high correlation between two covariates was observed, only the most relevant one from a physiological point of view was selected. In a second step, EBEs (Empirical Bayes Estimates) *versus* covariates were explored visually and a set of promising or clinically relevant covariates were selected. Finally the stepwise covariate model (scm) building procedure (26) that is automated in the software PsN (27) was used to obtain the statistically significant covariates. The scm procedure is based on an initial forward inclusion approach until the full covariate model is generated, followed by a backward deletion approach, deleting from the model those covariates that despite of being selected during the forward search do not match the statistical criteria. During the forward inclusion and backward deletion approaches the levels of significance used to incorporate to the model and to keep a covariate in the model were 0.05 and 0.01, respectively.

Model evaluation. Parameter precision was calculated from 1,000 nonparametric bootstrap analyses in PsN (27). Model performance was evaluated exploring visually

the goodness of fit plots including the conditional weighted residuals (CWRES) (28). Simulation-based diagnostics were also performed to further evaluate the selected model. One thousand data sets of the same characteristics of the original dataset were simulated and prediction-corrected visual predictive checks (pcVPCs) (29) were constructed and displayed graphically using PsN. Model performance at the individual level was evaluated to visually compare the raw and individual model predictions for the best, median, and worse fit patients, selected based on the mean value of the absolute prediction error calculated for each patient. Prediction error (PE) was computed as $[(C_{pred}\text{-}C_{obs})/C_{obs}]\times 100$, where C_{pred} and C_{obs} are the predicted and raw concentration values in plasma or in blood, respectively.

Model Exploration

The disposition model described by Eqs. 3 and 4 above implies that the ratio between C_B and C_P [blood to plasma ratio (BPR)] is not constant. Taking into account the following expressions it becomes clear that a dose dependent BPR value can have implications on the bioavailability: $F_H = 1\text{-}E_H$, $E_H = CL_B \times Q_H^{-1}$, and $CL_B = CL_P \times BPR^{-1}$, where CL_B, and CL_P are the apparent total blood and plasma clearance, respectively. F_H, refers to the (unknown) fraction of the absorbed dose that is lost during the first pass through the liver, and Q_H, corresponds to the liver blood flow. CL_P was calculated as k_{el} multiplied by V_P, and it was found to remain unchanged in the dose range studied (see results below).

To explore the effect of the non-linear uptake of irosustat by RBC on CL_B and F_H, calculations were made at the typical model predicted maximum C_B and C_P values at each dose level, assuming that liver metabolism is the major elimination route of irosustat.

RESULTS

Base Population Model

During model building different structural models for the different processes (absorption, distribution and elimination) were explored, as well as different relationships between plasma and blood irosustat profiles. First and zero order absorption models provided a worse description of the data compared to the performance of the transit compartments model. Multi-compartmental disposition models (e.g., two-compartment model) resulted not significantly better than the selected one compartment model ($p > 0.05$). Ignoring the limited binding capacity of the red blood cells resulted in a poor description of the data, especially for C_B. The typical estimate of A_{MAX} could not be obtained precisely, and therefore the following parameterization was used to improve parameter identifiability $K_D = A_{MAX}/SLP$ (30), where A_{MAX} and SLP are the parameters being estimated. Non-linear dose-dependent elimination was also explored during model building, but resulted not significant in the dose range studied. Model including time-variant parameters were also tested but data description was not improved significantly ($p > 0.05$).

Variability was supported on MTT, NTC, K_A, V_P, A_{MAX}, k_{el}, and F_1. However, after exploration of parameter precision by a nonparametric bootstrap analysis, a wide confidence interval for ISV on V_P was obtained suggesting that this random effect could not be precisely estimated. Off-diagonal elements of the Ω variance-covariance matrix and IOV were also explored, and resulted both non-significant ($p > 0.05$) except for the ISV of K_A and F_1 were a negative correlation was found.

Covariate Model

After a first visual screening (η-shrinkage below 30%) the following set of covariates were selected to further study their effects: HCT and WGT on k_{el}; dose level on F_1 and K_A; HCT, neutrophil counts, and WGT on MTT. Additionally, CYP2C9, CYP2C19, CYP3A5, CRCL, ALB, AGE, WGT were explored for significant effects on k_{el}, and F_1. After the scm analysis the only covariate relationship that resulted significant was the dose level on F_1.

Final Model Evaluation

Table II lists the estimates of the population pharmacokinetic parameters corresponding to the final selected model for irosustat administered orally. Although large confidence intervals were obtained for some ISV parameters, in general, parameters were obtained with reasonable precision based from the results obtained from the bootstrap analysis. ε-shrinkage was low for both plasma and blood observations (6.3 and 4.4% respectively), which means that the individual predictions *vs* individual observations plots are reliable. Goodness-of-fit plots for both type of measurements can be found on supplementary figure S1. Not apparent tendencies with respect to time and dose could be detected in any of the plots indicating good model performance. Lower panels of both figures also suggest (i) that the model captured very well the dose effects on the pharmacokinetics of irosustat (left) and (ii) the absence of time dependencies (right). Individual model predicted profiles corresponding to the worst, middle, and best fits are presented in supplementary figure S2.

Results of the simulation-based diagnostics (pcVPCs) showed that, in general, the model was able to describe

Table II Population Pharmacokinetic Parameter Estimates of Irosustat After Oral Administration

Parameter	Estimate (CV%)	[5th-95th]	ISV (%)	[5th-95th]
k_{el} (day^{-1})	4.08 (18)	[3.41–4.48]	25.6 (67)	[17.6–31]
V_B/F_1(L)	4.4 (15)	[3.84–4.81]	Ne	–
V_P/F_1(L)	294 (18)	[290–337]	12.2 (145)	[0.2–27]
K_A (day^{-1})	18.7 (33)	[13.2–26.7]	77.1 (59)	[41.8–104]
$F_1 = \theta_{F1} x$ (DOSE/40)$^{\theta DOSE}$	$\theta_{F1} = 1$ FIX $\theta_{DOSE} = -0.206$ (24)	– [−0.29−(−0.07)]	32.4 (41)	[19.5–40.6]
MTT (days)	0.0322 (33)	[0.0247–0.041]	66.1 (77)	[51.1–77]
NTC	3.05 (69)	[2.41–3.97]	57.8 (65)	[32.1–84.7]
A_{MAX} (mg)	51.6 (41)	[37.4–67.6]	68.5 (151)	[15–100]
SLP	5.35 (23)	[4.37–5.89]	Ne	–
K_D [1] (mg)	9.64	[7.36–14.1] [2]	–	–
$\omega^2_{KA,F1}$ [3]	−0.23 (52)	[−0.45−(−0.16)]	–	–
Residual error$_{Plasma}$ [log (ng/mL)]	0.55 (2)	[0.316–0.799]	Ne	–
Residual error$_{Blood}$ [log (ng/mL))]	0.545 (3)	[0.501–0.602]	Ne	–

Parameters are defined in the text; ISV; inter-subject variability expressed as coefficient of variation; Ne, not estimated; results from the bootstrap analysis are shown in brackets and summarizing providing the 5th and 95th percentiles; [1], Derived parameter calculated as A_{MAX}/SLP; [2], confidence intervals obtained from the bootstrap analysis; [3], typical value for correlation = 0.9

reasonably well the median tendency of the data (Fig. 3, where a data point was excluded from the lower right panel for better inspection) together with the non-linear uptake by the red blood cells (Fig. 4). There is however a tendency to overpredict the variability seen in the data. In addition, and to allow a better model evaluation, visual predictive checks have also been stratified by dose in both plasma and blood (supplementary figure S3).

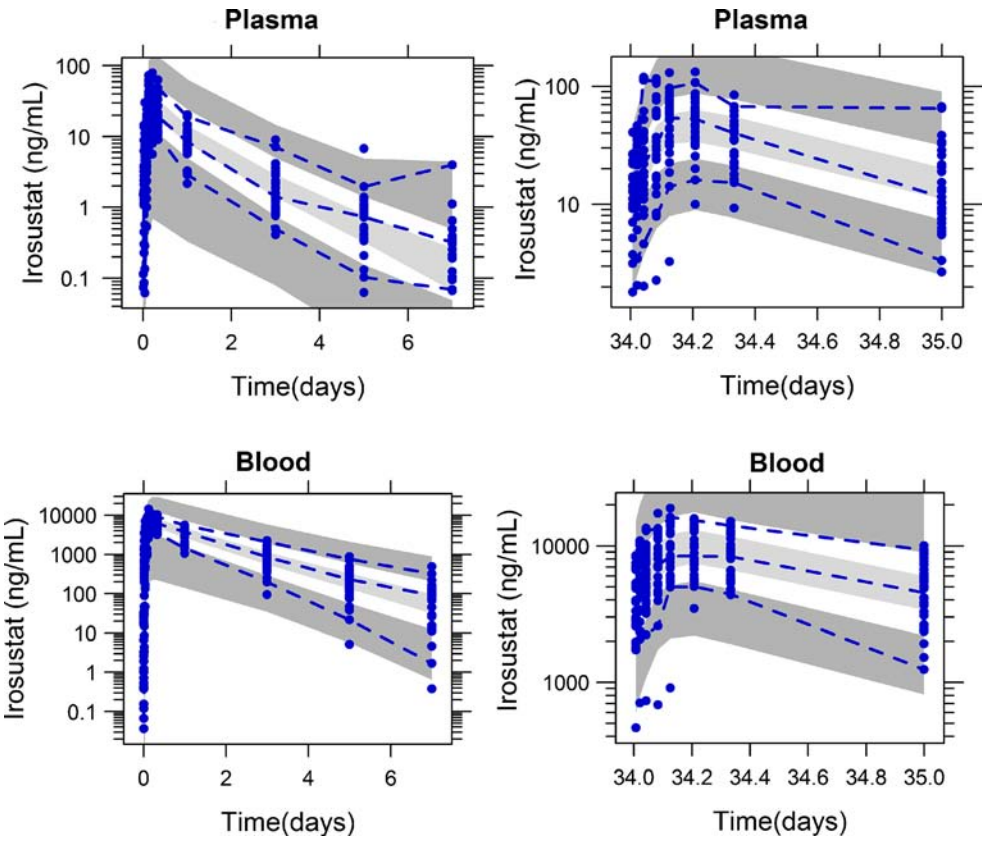

Fig. 3 Evaluation of the selected population pharmacokinetic model. Prediction- corrected VPC for plasma and blood profiles after the first (*left panels*) and last (*right panel*) administered doses. *Grey* areas represent the 90th prediction intervals of the 5th, 50th and 95th percentiles obtained by simulating 1,000 studies. *Blue points* are the prediction corrected observations and *dotted blue lines* represent the 5th, 50th and 95th percentiles calculated from the raw data.

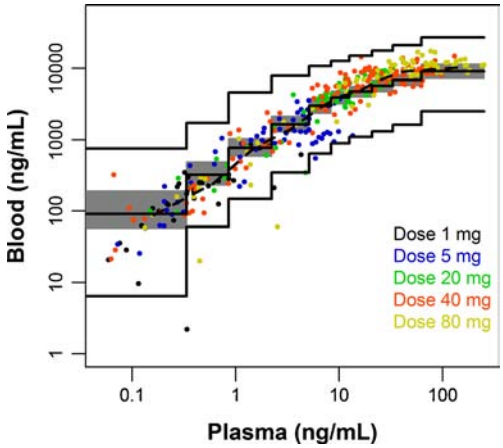

Fig. 4 Evaluation of the selected full population pharmacokinetic model with respect to the uptake process of irosustat by the red blood cells. *Grey area* represents the 90th prediction intervals of the 50th percentile obtained by simulating 1,000 studies. The *solid black lines* represent the 5th, 50th, and 95th percentiles of the simulated data. *Points* represent observation where each colour correspond to a dose level administered and the *dashed line* shows the median of raw data.

Simulated typical profiles of irosustat in blood and plasma for different dosing levels (Fig. 5) showed that despite the one compartment kinetics, and due to the saturable binding in the blood compartment, a non-linear decay for the highest simulated doses could be observed. Those typical simulated profiles indicate that doses lower than 20 mg irosustat show linear pharmacokinetic properties.

Model Exploration

Left panel in Fig. 6 shows the maximum typical C_P and C_B values (normalized to the typical value predicted for the 1 mg dose and corrected by predicted bioavailability) *versus* the corresponding dose level in log-log scale. It becomes clear that the increments in C_P and C_B with the dose are higher and lower than expected from a linear behaviour (solid line in black), respectively.

Middle panel of the same figure, the BPR and CL_B against dose profiles are shown. The BPR decreases with the dose level and consequently the CL_B is increased. Within the dose range administered in the current study CL_B typically passes from 2.5 at the 1 mg dose to 6 Lxh^{-1} at the 80 mg dose. Despite this more than two-fold impact of CL_B, the expected fraction of the dose lost during the first pass effect is almost negligible. F_H was typically estimated as 0.9985 for the 1 to 20 mg doses, and 0.998 and 0.997 for the 40 and 80 mg dose levels, using a value for the perfusion into the liver of 2,160 $Lxday^{-1}$. Right panel in Fig. 6 shows the individual predicted relative bioavailability estimates *versus* dose, together with the typical profile obtained from the covariate model selected. The plot reflects a misspefication of the covariate model for the 5 and 20 mg.

DISCUSSION

A population pharmacokinetic model capable to describe simultaneously the concentrations of irosustat in plasma and blood over time after single and repeated oral doses in postmenopausal women with oestrogen-receptor positive breast cancer has been developed and evaluated for a dosing range from 1 to 80 mg. In previous preliminary analysis, irosustat exhibited concentration-dependent pharmacokinetics (17) explained by a saturable distribution to the red cells for the higher studied doses, as could be observed in Fig. 1b. The model developed captured very well such non-linear behavior by considering instantaneous and reversible binding with limited distribution capacity (A_{MAX}) of the free drug to the red blood cells (Fig. 2).

From the current analysis, the value of the blood to plasma concentration ratio (BPR) in linear conditions can be derived.

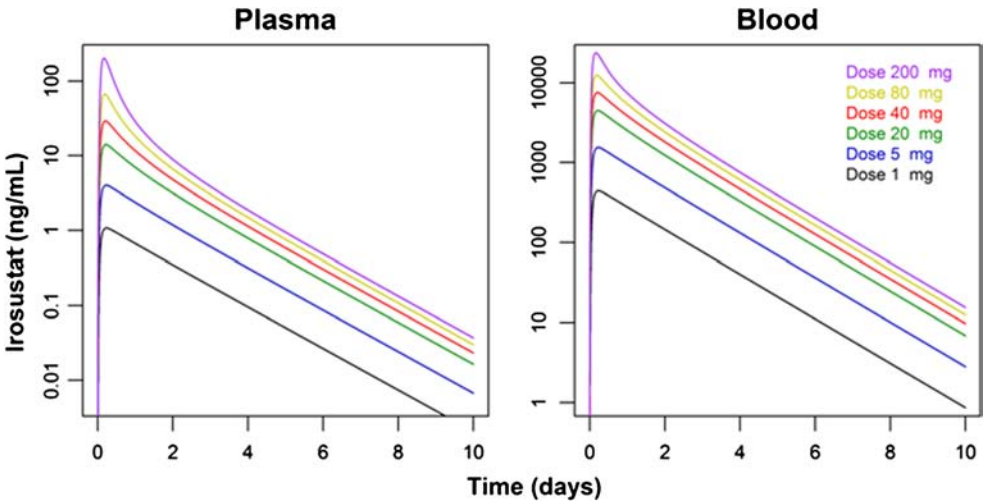

Fig. 5 Typical simulated population concentration profiles in plasma and blood after a single oral administration of different doses of irosustat.

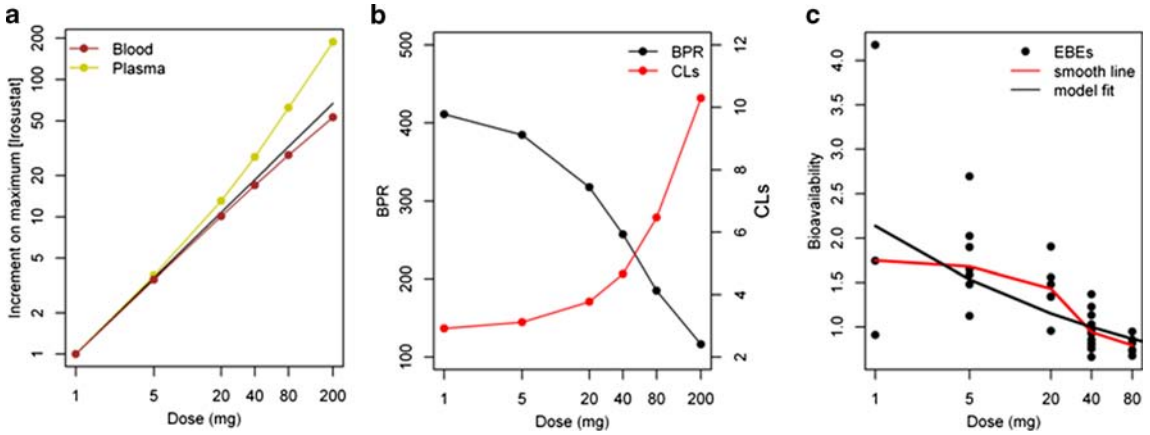

Fig. 6 Typical model predicted increments in maximum plasma and blood concentrations with respect to the 1 mg dose and normalized by the typical estimated of bioavailability. *Solid line in black* represents the relationship corresponding to linear, concentration-independent, disposition characteristics (*left*). Typical model predicted profiles corresponding to the blood to plasma concentration ratio (BPR) and apparent total blood clearance (*middle*). Empirical Bayes estimates (EBEs) of relative bioavailability *versus* the dose level administered (*points*). The *solid lines* represent the typical relationship predicted by the covariate model selected (*black*) and the general tendency of the data (*red*) (*right*).

Based on the results from the model developed, irosustat exhibits linear disposition properties at values of C_P lower than 32.79 ng/mL calculated as K_D/V_P (see value in Table II). At a C_P level of 5 ng/mL, the typical model predicted maximum blood concentration after the first dose equals to 1,537 ng/mL, and BPR is 307.4, indicating very high affinity for the red blood cells compartment.

Similarly, assuming only hepatic drug elimination, a total clearance of 1199.52 L/day (752–1852; 5th-95th range of distribution obtained from 1,000 simulations) can be obtained from the parameters listed in Table II representing the elimination clearance based on plasma concentration data. The corresponding blood clearance would be equal to 3.9 $L \times day^{-1}$, calculated as CL_{PL}/BPR, and under linear pharmacokinetic conditions. Those results might also indicate that irosustat is a low cleared drug. Nevertheless, it should be born in mind that given the lack of intravenous data, a complete oral bioavailability was assumed, which could hamper the physiological interpretation of all apparent volumes of distribution and clearance parameters.

Regarding the half-life, using Eq. 5 and final estimated parameters, a terminal slope of 0.64 $days^{-1}$ (approximately 25 h) is obtained in agreement with previously reported results (17). The estimate of the apparent volume of distribution in blood is 4.4 L which implies that if bioavailability is overestimated (i.e., lower than 1) V_B would be less than 4 L which is not physiologically possible. Model misspecifications in the characterization of the binding parameters as a results of the limited concentration range can be responsible of the resulted estimated of V_B/F_1.

Irosustat showed a low to moderate inter-subject variability (12–77%) in its absorption and disposition related parameters. Absorption parameters were associated to higher variability, an expected result taking into the limited solubility of the compound. Inter-subject variability can be present in the drug release processes represented by K_A, MTT and NTC. Variability in bioavailability was also estimated (32.4%).

In the current evaluation, a covariate analysis was performed. Remarkably neither the demographics (i.e., AGE, WEIGHT) nor the phenotypes for CYP2C9, CYP2C19, and CYP3A5 enzymes showed statistically significant effects. It should be noted here that, with exception of creatinine clearance, most of the bio-analytical measurement were within the normal ranges, preventing detection of covariate effects, and therefore, careful extrapolation of this results to a more critical population should be performed. The lack of effects of haemoglobin and hematocrit on the A_{MAX} and K_D parameters could be also explained due to the narrow interval of those covariates, but in addition, due to poor estimation of A_{MAX} and its inter-subject variability, possibly as a consequence of the limited range in the concentrations. However it was found that bioavailability decreased non-linearly as the administered dose increased. The selected covariate model predicts a 53, 33, 15%, increase in F_1 at doses of 5, 10, and 20 mg with respect to the median dose value of 40 mg. For the case of the highest dose administered, 80 mg, F_1 was 13.3% decreased with respect to the 40 mg dose.

In general, the model shows good overall performance in the dosing range studied (5–80 mg) providing reasonable pharmacokinetic parameter estimates. However, certain under-prediction was observed, especially in plasma, after the last irosustat administration. IOV was tested in the different model parameters, but it resulted not significant, suggesting that some time dependent processes that were not possible to identify are taking place. Further studies are needed in order to proper characterize this process.

Different mechanisms can be hypothesized to explain the decrease in bioavailability as the dose is augmented. Results

from the model exploration exercise, where the values of CL_B and F_H were studied over the dose range, showed that the increase in CL_B has a minimal impact on the bioavailability due to the first pass effect, and that the dose effect found on the relative bioavailability has to be mainly due to a limitation of the absorption process. A negative correlation of 0.9 was found (see Table II) between the first order rate constant of absorption and relative bioavailability. Preliminary data with different formulations showed that increasing the solubility of irosustat was associated to a lower bioavailability due probably to an instability of the drug in the gastrointestinal tract (data not shown). Another possibility is that drugs such as irosustat with a sulfamate moiety are sequestered by RBC after absorption (16), this binding protects them from the first pass metabolism when travelling through the liver. This mechanism could explain the decreased on F_1 with dose where the binding to RBC is saturated.

One possibility when dealing with concentrations of drug in plasma and blood is to develop a model for C_P and then use the following expression to get the predictions corresponding to C_B: $C_B = C_P \times (1\text{-HTC}) + C_{RBC} \times HTC$, where C_{RBC} represents the (unobserved) drug concentration in the red blood cells, which is predicted as $C_{RBC} = B_{MAX} \times C_P / (K_B + C_P)$, B_{MAX} is the maximum concentration of binding sites and K_B, represents the concentration of drug required to achieve 50% of B_{MAX} (31). However this approximation makes the assumption that the interaction between drug in plasma and red blood cells occurs within the plasma volume, which is not the case; the volume in which such process occurs is V_B not V_P. The modelling framework that is proposed in the current investigation takes into account the different volumes in which the different processes are taken place (i.e., elimination, distribution, and binding) which we think represents a more physiologic approach. The selected model deviates from Wagner's model where it is assumed that the binding and dissociation of drug molecules to tissue takes place in plasma. *A model taking into account the diffusion process between plasma and red blood cells as reported previously by Piekoszewski et al., (31) was also fit, but the current data did not support the estimation of the diffusion parameter. The structure of the model including diffusion process between plasma and red blood cells is represented mathematically in supplementary material figure S4.*

During the model development process we used the above mentioned approximation obtaining a two-compartment disposition model, with an unreasonable low estimate of V_P, and a covariate model describing an increase in K_A as the dose level was increased. Data description obtained from that model was very similar to that shown in Figs. 3 and 4, and supplementary figure S1 and S2. The selected model is simpler, with one parameter less to be estimated and provided a more meaningful estimate of V_P, and a more plausible effect of dose on the absorption process.

In summary, a population pharmacokinetic model of irosustat to simultaneously describe in a semi-mechanistic manner plasma and blood concentrations has been successfully developed by incorporating maximum distribution capacity of drug to red blood cells and a dose-dependent bioavailability with a predicted 47% decrease in relative bioavailability in the 40 mg with respect to the 1 mg dose. Based on the current results, irosustat shows linear dose independent characteristics at doses lower than 20 mg. The impact of the non-linear binding capacity on the plasma and whole blood pharmacokinetic profiles is minor at the recommended dose of 40 mg. During the treatment period irosustat showed time-independent pharmacokinetics. Pharmacokinetic processes of irosustat show low to moderate inter-subject variability, and neither the demographics (i.e., AGE, WEIGHT) nor the phenotypes for CYP2C9, CYP2C19, and CYP3A5 enzymes showed statistically significant effects.

ACKNOWLEDGMENTS AND DISCLOSURES

This work was financially supported by IPSEN Pharma

Zinnia Parra-Guillén and Iñaki F. Trocóniz received research financial funding from IPSEN Pharma

Josep María Cendrós Carreras, Concepción Peraire, Rosendo Obach, and Joan Prunynosa are past employees of IPSEN Pharma

Eric Chetaille is employee of IPSEN Pharma

REFERENCES

1. Ferlay J, Shin H, Bray F, Forman D, Mathers C, Parkin DM. Estimates of worldwide burden of cancer in 2008: GLOBOCAN 2008. Int J Cancer. 2010;127:2893–917.
2. Siegel R, Naishadham D, Jemal A. Cancer statistics, 2013. CA Cancer J Clin. 2013;63:11–30.
3. Barone I, Brusco L, Fuqua SAW. Estrogen receptor mutations and changes in downstream gene expression and signaling. Clin Cancer Res. 2010;16:2702–8.
4. Geisler J. Breast cancer tissue estrogens and their manipulation with aromatase inhibitors and inactivators. J Steroid Biochem Mol Biol. 2003;86:245–53.
5. Reed MJ, Purohit A, Woo LWL, Newman SP, Potter BVL. Steroid sulfatase: molecular biology, regulation, and inhibition. Endocr Rev. 2005;26:171–202.
6. Dowsett M, Goss P, Powles T, Hutchinson G, Brodie A, Jeffcoate S, *et al.* Use of the aromatase inhibitor 4-hydroxyandrostenedione in postmenopausal breast cancer: optimization of therapeutic dose and route. Cancer Res. 1987;47:1957–61.
7. Santner SJ, Feil PD, Santen RJ. In situ estrogen production via the estrone sulfatase pathway in breast tumors: relative importance versus the aromatase pathway. J Clin Endocrinol Metab. 1984;59:29–33.
8. Reed M, Lai L, Owen A, Singh A, Coldham N, Purohit A, *et al.* Effect of treatment with 4-hydroxyandrostenedione on the peripheral conversion of androstenedione to estrone and in vitro tumor aromatase activity in postmenopausal women with breast cancer. Cancer Res. 1990;50:193–6.
9. Noel C, Reed M, Jacobs H, James V. The plasma concentration of oestrone sulphate in postmenopausal women: lack of diurnal

variation, effect of ovariectomy, age and weight. J Steroid Biochem. 1981;14:1101–5.
10. Purohit A, Dauvois S, Parker M, Potter B, Williams G, Reed M. The hydrolysis of oestrone sulphate and dehydroepiandrosterone sulphate by human steroid sulphatase expressed in transfected COS-1 cells. J Steroid Biochem Mol Biol. 1994;50:101–4.
11. Utsumi T, Yoshimura N, Takeuchi S, Maruta M, Maeda K, Harada N. Elevated steroid sulfatase expression in breast cancers. J Steroid Biochem Mol Biol. 2000;73:141–5.
12. Suzuki T, Nakata T, Miki Y, Kaneko C, Moriya T, Ishida T, *et al.* Estrogen sulfotransferase and steroid sulfatase in human breast carcinoma. Cancer Res. 2003;63:2762–70.
13. Purohit A, Woo LW, Potter BV, Reed MJ. In vivo inhibition of estrone sulfatase activity and growth of nitrosomethylurea-induced mammary tumors by 667 COUMATE. Cancer Res. 2000;60:3394–6.
14. Foster PA, Newman SP, Chander SK, Stengel C, Jhalli R, Woo LL, *et al.* In vivo efficacy of STX213, a second-generation steroid sulfatase inhibitor, for hormone-dependent breast cancer therapy. Clin Cancer Res. 2006;12:5543–9.
15. Ventura V, Solà J, Celma C, Peraire C, Obach R. In vitro metabolism of irosustat, a novel steroid sulfatase inhibitor: interspecies comparison, metabolite identification, and metabolic enzyme identification. Drug Metab Dispos. 2011;39:1235–46.
16. Ventura V, Solà J, Peraire C, Brée F, Obach R. In vitro evaluation of the interaction potential of irosustat with drug-metabolizing enzymes. Drug Metab Dispos. 2012;40:1268–78.
17. Coombes RC, Cardoso F, Isambert N, Lesimple T, Soulié P, Peraire C, *et al.* A phase I dose escalation study to determine the optimal biological dose of irosustat, an oral steroid sulfatase inhibitor, in postmenopausal women with estrogen receptor-positive breast cancer. Breast Cancer Res Treat. 2013;140:73–82.
18. Ireson C, Chander S, Purohit A, Parish D, Woo L, Potter B, *et al.* Pharmacokinetics of the nonsteroidal steroid sulphatase inhibitor 667 COUMATE and its sequestration into red blood cells in rats. Br J Cancer. 2004;91:1399–404.
19. Beal S, Sheiner L, Boeckmann A. NONMEM Users Guide. 1989–2006.
20. Karlsson M, Sheiner L. The importance of modeling interoccasion variability in population pharmacokinetic analyses. J Pharmacokinet Biopharm. 1993;21:735–50.
21. Ludden TM, Beal SL, Sheiner LB. Comparison of the Akaike information criterion, the Schwarz criterion and the F test as guides to model selection. J Pharmacokinet Pharmacodyn. 1994;22:431–45.
22. Savic RM, Jonker DM, Kerbusch T, Karlsson MO. Implementation of a transit compartment model for describing drug absorption in pharmacokinetic studies. J Pharmacokinet Pharmacodyn. 2007;34:711–26.
23. Wagner JG. A new generalized nonlinear pharmacokinetic model and its implications. In: Wagner JG, editor. Biopharmaceutics and relevant pharmacokinetics: drug intelligence publications. 1971. p. 302–17.
24. Picard-Hagen N, Gayrard V, Alvinerie M, Smeyers H, Ricou R, Bousquet-Mélou A, *et al.* A nonlabeled method to evaluate cortisol production rate by modeling plasma CBG-free cortisol disposition. Am J Physiol Endocrinol Metab. 2001;28:E946–56.
25. Mager DE, Mascelli MA, Kleiman NS, Fitzgerald DJ, Abernethy DR. Simultaneous modeling of abciximab plasma concentrations and ex vivo pharmacodynamics in patients undergoing coronary angioplasty. J Pharmacol ExpTher. 2003;307:969–76.
26. Jonsson EN, Karlsson MO. Automated covariate model building within NONMEM. Pharm Res. 1998;15:1463–8.
27. Lindbom L, Pihlgren P, Jonsson N. PsN-Toolkit—A collection of computer intensive statistical methods for non-linear mixed effect modeling using NONMEM. Comput Methods Prog Biomed. 2005;79:241–57.
28. Hooker AC, Staatz CE, Karlsson MO. Conditional weighted residuals (CWRES): a model diagnostic for the FOCE method. Pharm Res. 2007;24:2187–97.
29. Bergstrand M, Hooker AC, Wallin JE, Karlsson MO. Prediction-corrected visual predictive checks for diagnosing nonlinear mixed-effects models. AAPS J. 2011;13:143–51.
30. Schoemaker RC, van Gerven JM, Cohen AF. Estimating potency for the E max-model without attaining maximal effects. J Pharmacokinet Biopharm. 1998;26:581–93.
31. Piekoszewski W, Chow FS, Jusko WJ. Disposition of tracolimus (FK 506) in rabbits. Role of red blood cell binding in hepatic clearance. Drug Metab Dispos. 1993;21:690–8.